Exploitation of liquid CO2 based greener process for valorization of citronellal rich essential oils into flavor grade (-)-menthol using novel Sn/Al-B-NaYZE composites

Prashant Kumar
Central Institute of Medicinal and Aromatic Plants CSIR https://orcid.org/0000-0001-6594-7930
Chandan Singh Chanotiya
Central Institute of Medicinal and Aromatic Plants CSIR https://orcid.org/0000-0001-9802-0162
Laldingngheti Bawitlung
Central Institute of Medicinal and Aromatic Plants CSIR
Anju Yadav
Central Institute of Medicinal and Aromatic Plants CSIR
Pankaj Kumar
Central Institute of Medicinal and Aromatic Plants CSIR
Anirban Pal
Central Institute of Medicinal and Aromatic Plants CSIR
Ajit Kumar Shasany
Central Institute of Medicinal and Aromatic Plants CSIR
Priyabrat Mohapatra
C V Raman Global University https://orcid.org/0000-0002-6750-6271
Prasant Kumar Rout (pk.rout@cimap.res.in)
Central Institute of Medicinal and Aromatic Plants CSIR https://orcid.org/0000-0003-3018-3357

Research Article

Keywords: (-)-Menthol, Liquid CO2, Composites, Sn-B-NaYZE, 14C-Biobased index, Bioactivity

Posted Date: July 29th, 2022

DOI: https://doi.org/10.21203/rs.3.rs-1827388/v1

Abstract

A two-step greener catalytic process has been developed for semi-synthesis of (-)-menthol from citronellal-rich essential oils such as *Cymbopogon winterianus* and *Corymbia citriodora* by using novel bi-acidic composites. These novel composites (Al-B-NaYZE or Sn-B-NaYZE) were prepared by impregnation of Sn-B and Al-B over NaYZE framework to increase the Lewis and Bronsted acidic sites. These composites were thoroughly characterized using TDP, FT-IR, UV, XRD, SEM, HRTEM, SA, and TGA. The composite Sn-B-NaYZE cyclized 99% of citronellal to isopulegol isomers with 99% selectivity in 45 min under liquid CO_2 medium, while composite Al-B-NaYZE is showing 95% selectivity towards isopulegol isomers. Sn-B-NaYZE was displayed ehnaced selectivity due to its higher acidic property as confirmed by the TPD analysis. The chiral study indicates that the Sn-B-NaYZE composite is giving highest selectivity (94%) towards (-)-isopulegol. (+)-Citronellal or citronellal oil was found as an ideal substate for (-)-menthol production. It observed that Sn-B molar ratio over base material NaY-Zeolite was played a mojor role for catalytic activity and selectivity towards (-)-isopulegol. Further, isopulegol isomers were reduced to 98% of menthol using 1%Pd/AC at 40 psi H_2 pressure in 1 h. Reaction mixture slowly frozen to -40^oC for trouble-free isolation of the crude menthol. Further, pharmaceutical and flavor grade (-)-menthol was purified from the crude menthol through esterification process. This (-)-menthol was found to 100% biobased on ^{14}C-radiocarbon-dating to authenticate as nature-identical. The composite has displayed high reusability up to five times without significant loss in their activity. After isolation of menthol, the spent oil was enrich with oxygenated monoterpenoids, hence it was displayed significant antimicrobial activities.

Statement Of Novelty

A two-step greener catalytic process has been developed for semi-synthesis of (-)-menthol from citronellal-rich essential oils using novel bi-acidic composites. The composite Sn-B-NaYZE cyclized 99% of citronellal to isopulegol isomers with 99% selectivity in 45 min under liquid CO_2 medium, while composite Al-B-NaYZE is showing 95% selectivity towards isopulegol isomers and this is due to higher acidic property of Sn-B-NaYZE. The chiral study indicates that the Sn-B-NaYZE composite is giving highest selectivity (94%) towards (-)-isopulegol. Sn-B molar ratio over base material NaY-Zeolite have displayed a significant catalytic activity and selectivity towards (-)-isopulegol. This isopulegol isomers were reduced to 98% of menthol using 1%Pd/AC at 40 psi H_2 pressure in 1 h. Further, pharmaceutical and flavor grade (-)-menthol was purified and this (-)-menthol was found to 100% biobased on ^{14}C-radiocarbon-dating to authenticate as nature-identical. After isolation of menthol, the spent oil was enrich with oxygenated monoterpenoids, hence it was displayed significant antimicrobial activities. The present study provides the eco-friendly greener process for direct valorization of citronellal rich essential oils.

Introduction

(-)-Menthol crystal is a food-flavor and pharmaceutically important compound with several applications in chewing gums, mouth fresheners, ointment, syrup, aromatherapy, and flavoring the food products, etc [1, 2]. This is an excellent palatable molecule to use as a food-preservative at low concentration without much altering the sensory value of the food products [3, 4]. Naturally, menthol is obtained from *Mentha arvensis* or

Mentha piperita (Family *Lamiaceae*) essential oil through crystallization at a low temperature (<-40 ^{o}C) [5]. Major menthol producing countries are India, China, USA, Japan, Australia, Argentina, Brazil, Hungary, France, Czechoslovakia, Italy, Paraguay, etc. (-)-Menthol is the major compound (65–85%) of *M. arvensis* essential oil [6]. The mentha oil (26,000 Ton) production is the Worlds' second most essential oil after orange oil with its trading value of 34.4 x 10^6 USD [7]. Though 60% of (-)-menthol crystal is produced from natural sources of this essential oil, the remaining is manufactured by chemical synthesis methods. The commercial processes were reported using non-environmentally friendly catalysts such as $ZnBr_2$, BF_3, $SbCl_3$, $TiCl_4$, etc with about 70% of yield [8, 9]. The transformation of citronellal to isopulegol was also reported using SiO_2, TiO_2, ZrO_2, FeF_3-MgF_2, 1.5%Pd-20%PW/SiO_2, etc in organic solvents [8, 10]. These processes gave up to 90% yield with inferior selectivity of key isomer (isopulegol) at high temperature (up to 250 ^{o}C), and H_2 pressure (5–50 bar).

The reported processes might be clear-cut for menthol conversion when using the pure (+)-citronellal as substrate. But, the major challenge arises, when this conversion is attempted in essential oils containing an enantiomeric mixture of (±)-citronellal. The selective transformation of citronellal in the essential oil is a challenging task due to the presence of a large number of thermolabile terpenoids. As a result, either the catalytic active sites have been reduced or constituents other than the target compound are chemically transformed. Therefore, effective catalysts for selective conversion are of utmost importance to get the economically viable process. The present work overcomes such limitations using inexpensive composites at a lower temperature, and atmospheric pressure conditions have been facilitated for the production of menthol directly from low-value essential oils. Hence, presently the preparation of menthol from crude citronellal-rich essential oils (feedstocks) such as citronella, eucalyptus, etc has been carried out. Since, the essential oils are contained enantiomeric mixtures of (±)-citronellal, hence enatiospecific semi-synthesis of isopulegol has been studied. The present process is realized reasonably low-cost composites for the conversion of citronellal to isopulegol using Al-B-NaYZE or Sn-B-NaYZE in the first step using liquid-CO_2 solvent. Liquid CO_2 is a green and eco-friendly solvent system, and it is easily attained the liquid state at below critical condition (31.1 ^{o}C, 73.8 bar) of CO_2 [11]. Importantly, in the second step, isopulegol was reduced using a very low percentage of Pd or Ru to produce the menthol. In addition, (-)-menthol was isolated, purified, and validated through the biobased index to prove it as a nature-identical molecule. Purification of (+)-citronellal from essential oils is cost as well as labor-intensive, therefore the direct selective transformation and isolation of (-)-menthol is an attractive alternative. Besides (-)-menthol, the other compounds in the modified essential oil have been produced a better olfactometry profile to use as a fine fragrance and food additive in various industries.

Experimental

(+)-Citronellal, (-)-citronellal, (+)-isopulegol, (-)-isopulegol, (±)-menthol, (-)-menthol, $Pd(NO_3)_2$, $Ru(NO)(NO_3)_3$, activated charcoal (AC), $Al(NO_3)_3$, $Sn(SO_4)_2$, boric acid (BA), NH_4Cl, and common organic solvents were procured from Sigma-Aldrich, Bengaluru. Na-Y-Zeolite (NaYZE) was purchased from Thermo-Fischer chemicals, Hyderabad. Citronella (*Cymbopogon winterianus, var*. CIM-Jeeva, and BIO-13) ariel parts were harvested from CSIR-CIMAP, Lucknow research farm (26.87^{o}N, 80.98^{o}E), Uttar Pradesh, India. The essential oil was isolated from this biomass using the field distillation unit. On the other hand, eucalyptus (*Corymbia citriodora*) leaves were collected from the same research farm, and the essential oil was isolated using the

laboratory design distillation apparatus. The compositions of both the essential oils are determined by GC-FID and GC/MS. A detailed methodology is given in the Supplementary data.

Preparation of composites

Paste of NaYZE was made in distilled water and then the acidified molar solution of $Al(NO_3)_3$ or $Sn(SO_4)_2$ was impregnated at 30 ^oC with constant stirring (800 rpm) for 2 h. Thereafter, the materials were thoroughly washed with distilled water and kept for drying at 120 ^oC. The composites were powdered again and calcined at 550 ^oC to obtain Al-NaYZE or Sn-NaYZE. Then, aqueous BA was added drop-wise in the above mixture and stirred for 2 h at 30 ^oC to obtain the composites by the co-precipitation method. These composites were placed in an oven at 110 ^oC for complete evaporation of water. Then, composites were thoroughly washed in water followed by drying at 110 ^oC. Finally, these composites were calcined for 5 h at 550 °C to obtain Al-B-NaYZE or Sn-B-NaYZE. Further, YZE (Y-H-Zeolite) was produced from NaYZE by ion exchange with 2M NH_4Cl solution followed by washing, drying, and calcination at 550 ^oC. Then a similar methodology was followed for the preparation of Al-B-YZE or Sn-B-YZE composites. The molar ratio of each active component is given in Supplementary Table S1.

Reduced metal catalysts were prepared as follows: 100 mg of 10 mmol of $Pd(NO_3)_2$ or $Ru(NO)(NO_3)_3$ were dissolved in 30 mL of 1N HCl, and then an aqueous solution of $NaHCO_3$ was used to maintain the pH 7. Thereafter, 15-20 mL of $NaBH_4$ (0.05 mmol) and 15-20 mL of glucose (0.3 mmol) were added in stirring conditions for 30 min to obtain a colloidal solution. AC was added in appropriate amounts of Pd or Ru colloidal solution to achieve 0.5-2%Pd/AC or Ru/AC catalyst. Then, catalysts were thoroughly washed in water followed by drying at 110 ^oC. The dried catalyst was placed in a furnace at 220 ^oC for 4 h before use. Similarly, the other reduction catalysts are prepared as per Supplementary Fig. S1.

Characterization of catalysts

Catalysts were characterized using UV-Vis, FT-IR, XRD, SA (surface area), NH_3-TPD, SEM-EDX, TEM, HRTEM-EDX, TGA, XPS, True density, and ICP-OES as per the protocol given in Supplementary data. The Lewis and Bonsted acid sites in the composites are determined by the pyridine (Py)-TGA adsorption-desorption method (Supplementary data).

Reaction conditions

The citronellal cyclization (Prins Reaction) was carried out using cyclohexane, toluene, CH_2Cl_2 solvent system in a ratio of citronellal to solvent (5:1 to 8:1) in an RB flask connected to the condenser. Further, a ratio of composites to citronellal (1:15 to 1:18) was added into this reaction mixture. The mixture was allowed to agitate at a rate of 400 rpm at 50-75 ^oC for 15 min to 2 h. Finally, the process optimization was carried out using Al-B-NaYZE and Sn-B-NaYZE composites (Supplementary Table S2, and S3).

The above Prins Reaction of citronellal was carried out in a laboratory specially designed stainless steel liquid CO_2 apparatus. The experimental system for the liquid-CO_2 extraction unit has been illustrated in Supplementary Scheme S1. Citronellal (1 g) was taken in a designed beaker along with 70 mg of

composites (Al-B-NaYZE or Sn-B-NaYZE). The reaction was carried out at 21 ^{o}C (approx) with CO_2 pressure of 68-70 bar. The chilled water was circulated in the cooling figure of the apparatus at 15 ^{o}C and the bottom of the apparatus was maintained at 34 ^{o}C. The process of evaporation and condensation were repeated throughout the process for 15-45 min. Then the CO_2 was removed to obtain isopulegol isomers. Further, it was dissolved in ethanol and then filtered to obtain isopulegol solution. In the further scale-up study, citronellal (10 g) with 0.6 g of the composite were taken for the cyclization reaction under the same reaction conditions for 45 min. For direct conversion, 20 g of essential oil (Citronella or Eucalyptus) was taken with a ratio of citronellal-composite (10:0.7) for 45 min.

Again, the reacted-mixture in the above (first) step was reduced to menthol under H_2 pressure (10-40 psi) using prepared Pd/AC or Ru/AC catalyst in a ratio of 1:10 to 1:13 (catalyst: reacted mixture) in ethanol for 10 to 60 min (Supplementary Table S3, and S4). In a similar methodology, the above-reacted oil mixture was reduced using Pd/AC. After completion of step-two reaction, the ethanol was removed in a rotary evaporator at 50 ^{o}C under 150 mbar pressure, and then the modified oil was kept in a refrigerator at -40 ^{o}C for 24 h to isolate the crude menthol crystal. For enrichment of (-)-menthol, the crude menthol isomers were derivatized to menthyl acetate using acetic anhydride or acetyl chloride (Supplementary data). After completion of the reaction, (±)-menthyl acetate was crystallized at 35 ^{o}C to isolate (-)-menthyl acetate, whereas other diastereomers remained in the liquid phase. The hydrolysis of (-)-menthyl acetate was yielded (-)-menthol. Further, (-)-menthol was crystallized at -40 ^{o}C to obtain the bold crystals. The citronellal conversion is determined by using the Eqs. (1-3).

$$XCAL = \frac{Ccal^{o} - Ccal^{t}}{Ccal^{o}} \quad (1)$$

where $Ccal^{o} = initial\ concentration$, and $Ccal^{t} = concentration\ at\ time\ t$

Product selectivity (Si) is calculated as $Si = \frac{Ci}{\sum Ci}$ (2)

$$\sum Ci = total\ moles\ of\ product$$

The reaction rate (R) is calculated by $R = \frac{Change\ in\ the\ concentration\ of\ reactants\ (mol/l)}{Time\ taken\ (s)}$ (3)

Enantiomeric characterization

The enantiomeric ratios determination of citronellal oils and the reaction mixtures are carried out through chiral-GC-FID. For, ^{13}C-NMR spectrum, menthol (10 mg) was dissolved in $CDCl_3$ and recorded on DPX-500

Bruker system at 125 MHz at 26 ^{o}C with trimethylsilane (TMS) as the internal standard. The detailed enantiomeric characterization is given in the Supplementary data.

Biobased evaluation

Biobased evaluation of the samples is done by quantification of ^{14}C content, which is reported in the percentage of modern carbon (pMC) values. Accelerator Mass Spectrometry (AMS) facility at Inter-University Accelerator Centre, New Delhi was used for the quantification of biobased carbon content in each sample. Processed samples were combusted in automated graphitization equipment (AGE), and converted into graphite powder for enabling AMS measurements to quantify the ^{14}C/^{12}C ratio. An ion accelerator (500 kV) based AMS system was used for the quantification of ^{14}C/^{12}C present in each of the samples. Instrument details and measurement procedure was reported in our earlier publication [12].

Bioactivity

The bioactivities of essential oils and their modified oils have been studied. The detailed methodology of anti-microbial and antioxidant activities are given in the Supplementary data.

Characterization of spent catalysts

The reaction medium after filtration was used for the estimation of B, Al, Si, Sn, and Na. Before each experiment, the used composites were thoroughly washed with acetone as well as using water, and calcined at 550 ^{o}C for 5 h. There was not much difference in SA and porosity of the re-used composites. After filtration of composites, the reaction was terminated to justify the heterogeneous nature of the catalytic properties. A leaching test of the filtrate was performed by removing the composites from the reaction mixture after 45 min. Similarly, 1%Pd/AC was thoroughly washed with warm water (60 ^{o}C) and calcined at 220 ^{o}C for 4 h before synthesis using the next batch of reactions.

Results And Discussion

Characterization of essential oil

The yield of essential was obtained from *C. winterianus* (CIM-Jeeva: 1.2% and BIO-13: 1.3%) and *C. citriodora* (2.8%), respectively. Citronellal is a major compound in these essential oils and their compositions before and after conversion are presented in Table 1. Citronella oil was contained 38.9-41.4% of citronellal with (+)-citronellal (91%) as the predominant enantiomer followed by (-)-citronellal (9%). Whereas, eucalyptus oil was possessed 69.5% of citronellal with (-)-citronellal (48%) and (+)-citronellal (52%) in enantiomeric contour. In toxicity assay, citronellal was found to be a harmful compound (LC50: 0.04) as compared to menthol (LC50: 0.39) [13]. Therefore, menthol is the best-suited compound for pharmaceutical and nutraceutical applications.

Characterization of composites

The surface morphology of the composites (Sn-B-NaYZE, Al-B-NaYZE, Sn-B-YZE, and Al-B-YZE) were examined by SEM and TEM. The SEM micrograph revealed that all particles persist in a well shaped structure, size ranging from 0.54 to 0.78 µm (Fig. S2). Also, the SEM images of 1%Pd/AC and 1%Ru/AC have been shown the

proper incorporation of Pd and Ru on AC surface (Fig. S2c,f). TEM images of composites is present in Supplementary Fig. S3, and it reveals that the composites of Al-B-NaYZE and Al-B-YZE were homogeneous and smooth as compared to Sn-B-NaYZE and Sn-B-YZE. HRTEM images of Sn-B-NaYZE, which indicated the proper incorporation of metals (Sn, B) on NaYZE, the variant lattice pattern is indicated as polycrystalline nature, which is further confirmed by the SAED ring pattern (Fig. 1c). A high-resolution image suggested that the uniform distribution of sodium borate as black lines on the surface of Sn impregnated ZE. On the other hand, the HRTEM image of Al-B-NaYZE shows the high dispersion of particles. It was predicted that AlO and BO on NaYZE made the composite smooth to form indistinguishable morphology. In Sn-B-NaYZE, the HRTEM micrographs reveal the lattice constants of 0.25 nm and 0.35 nm were attributed to the plane of 101 and 110 of SnO_2 assigned to the *d* spacing. The lattice fringe of the HRTEM of SnO_2 was complimented well to the XRD data. Fig. 1f-l shows the individual maping of elements present in Sn-B-NaYZE composite. Moreover, the elemental distribution of composites is determined through SEM-EDAX analysis (Fig. S4 and S5). The obtained metal weight % was in correlation with XPS results.

XRD data of prepared catalysts Al-B-NaYZE, Sn-B-NaYZE, Al-B-YZE, and Sn-B-YZE were presented in Fig. S6. For Al-B-NaYZE and Sn-B-NaYZE, the 2θ values recorded at 6.1°, 11.8°, 15.5°, 20.2°, 23.4°, resemble the peaks observed in a typical NaYZE. These values of 2θ were matched to the hkl values of 111, 311, 331, 440, and 533, respectively [14,15]. The lack of any hump and soft horizontal line in the background was indicated the complete crystallinity in composites without any amorphous species (SiO_2) [16,17]. In Sn-B-NaYZE has been shown 2θ correspond to 26.4 and 33.9, these are matched with lattice planes of 110 and 101 of SnO_2, respectively [18]. The resemblance of XRD patterns of Sn-B-NaYZE and Sn-B-YZE have indicated the successful incorporation of Sn into the NaYZE and YZE framework, and it is supported by decreasing the molar ratio of SiO_2/Al_2O_3 in Sn-B-NaYZE and Sn-B-YZE (Table 2). Al/Sn impregnated ZE had reduced crystallinity in comparison to the normal one, which was reflected by decreasing the intensity of diffraction peaks. Sn-B-NaYZE was less crystalline as compared to Al-B-NaYZE and Na-YZE. The incorporation of Sn is led to enhance the Na content (Table 2). The conventional YZE framework was composed of SiO_4 and AlO_4 species, which were arranged in tetrahedral symmetry. Due to the different oxidation states of Al^{3+} and Si^{4+}, which were impacted the overall negative charge to the framework, thereby need monovalent ion (Na^+) for maintaining the charge balance. For Sn^{2+} composite, the framework has shifted the burden to increase the negative charge, hence additional monovalent Na^+ was needed for maintaining the charge neutrality to facilitate better incorporation of Sn^{2+} [16]. The intensity of characteristic peak was indicated the extent, as well as the concentration of crystallinity in composites could be expressed according to the equation described by Pal *et al* [19]. The absence of a any extra peak at 28^o was indicated that no more free BA in the composites [20]. Similarly, 1%Pd/AC has shown the characteristics 2θ peaks at 40.5^o, 47.0^o, and 68.5^o.

The data for NH_3-TPD of Al-B-Na-YZE, Sn-B-Na-YZE, Al-B-YZE and Sn-B-YZE depicted two peaks: one narrow peak at 150 ^{o}C and another broad peak at 500 ^{o}C. The low temperature peak was derived from the weakly adsorbed NH_3 molecules via H-bonding. Whereas, the high temperature peak was ascribed to strong Bronsted acid sites. As shown in Fig. 2a, the total peak area corresponding to Al-B-YZE, Sn-B-YZE, Al-B-Na-YZE and Sn-B-Na-YZE are 4326.2, 9600.6, 30369.0 and 41108.1 sq. unit respectively, which indicated that the Na composites have enhanced acidic character. Besides acidic character, Al-B-NaYZE and Sn-B-NaYZE have appeared

analogous to the cubic structure of aluminosilicate, which might be facilitated higher Bronsted acidic characteristics [21]. The relative abundance of Lewis acid concentrations at 150 ^{o}C were 7,334.1 and 1,241.6 sq. units for Al-B-NaYZE and Al-B-YZE, respectively. Similarly, the amounts of Bronsted acid concentrations at 500 ^{o}C were 22,290.9 and 3,082.4 sq. units for Al-B-NaYZE and Al-B-YZE, respectively. It is clear that Al-B-NaYZE is a strong acidic composite as compared to Al-B-YZE. Amounts of weak acid concentrations at 150 ^{o}C are 9,199.2 and 3,206.6 sq. units for Sn-B-NaYZE and Sn-B-YZE, respectively. Similarly, the amounts of strong acid concentrations at 500 ^{o}C are 30,572.1 and 6,365.2 sq. units for Sn-B-NaYZE and Sn-B-YZE, respectively. From the above results, Sn-B-NaYZE is a strong acidic composite as compared to Sn-B-YZE. The lower percentage of B loading was slightly impacted the Si/B ratio, which helped to shift the orientation towards the tetrahedral coordination. On the other hand, higher B loading was decreased the Si/B ratio, hence facilitating the trigonal forms of coordination [22]. Therefore a definite percentage of B incorporation has been shown to enhance the Prins reaction, due to its proper balance in between the trigonal and tetrahedral coordination forms. Trigonal B has represented the Lewis acidic character, whereas B is exhibited the Bronsted acidic behavior in dynamic equilibrium to favor the extra-ordinary activity of these composites [23].

The incorporation of Sn into the ZE (zeolite) framework is verified by examining the bands formed by charge transfer from ligand to the metal as analyzed from the UV-Vis spectra (Fig. 2b). Sn-B-NaYZE and Sn-B-YZE exhibited a strong UV-Vis characteristic absorption band centered at 219 nm, which was featured in the presence of tetracoordinate Sn^{4+} in the ZE framework. The intensity of this band was proportional to the loading of tetrahedrally coordinated Sn^{4+} ion.[23] The band at 250 nm was attributed to the polymeric SnO_2 species. Therefore, the stronger band intensity of Sn-B-NaYZE in comparison to that of the Sn-B-YZE suggested the greater formation of Sn^{4+} species during its incorporation procedure [24]. The absorption spectra of pure SnO_2 demonstrated an extensive band at ~240-400 nm, which was allocated to the polymeric Sn-O-Sn category species. The absorption spectra of Sn-B-NaYZE and Sn-B-YZE exhibited a blue shift relative to the pure SnO_2. This blue shift could be attributed to small SnO_2 species, and is largely dependent on the size-quantization of the SnO_2 particles in the nanometer regime. SnO_2 species were smaller in size and impacted a stronger blue shift [18]. The blue shift is more significant for Sn-B-NaYZE, which indicated the presence of smaller SnO_2 particles (Fig. 2b). The absorption spectrum of Sn-B-NaYZE has contained a strong band at ~205 nm with very weak shoulder bands in between ~290-420 nm. The findings indicated that most of the Sn was inserted into the tetrahedral framework, and very few of them were present in the extra framework. However, SnO_2 phases were not detected in Sn-B-YZE. Furthermore, the spectra of Al-B-NaYZE and Al-B-YZE were quite similar to YZE spectra, which means no such changes were observed after Al impregnation on the ZE framework.

XPS spectra of composites are presented in Supplementary Fig. S7. The XPS spectra illustrated two principal signals that related to Sn $3d^{5/2}$ and Sn $3d^{3/2}$ photoelectrons with binding energies of 487.0 and 495.5 eV, respectively (Fig. 2c), which indicated the existence of Sn^{4+} particles on the surface [23]. The count Sn-B-NaYZE was higher as compared to the Sn-YZE. The consequences implied that the Sn-B-NaYZE is acquired more framework of Sn particles on the surface, which is complied with the results of UV-Vis and SEM-EDX (Table 2). The peaks at the binding energy of 74.0, 74.8, 75.2, and 75.8 eV have confirmed the presence of Al-O and Al-OH (Al $2p^{3/2}$) species. The peaks of Al 2p (76.2) and Si 2p (103.3) are confirmed that these elements

are properly integrated with YZE in Sn-B-NaYZE and Al-B-NaYZE (Supplementary Fig. S7b). The counts of Al-B-NaYZE and Al-B-YZE are higher than that of Sn-B-NaYZE and Sn-B-YZE, which suggested the proper impregnation of Al on the ZE framework, and hence the presence of Al extra framework. The signal at 192.8 eV in all samples has confirmed the presence of B species in the form of B_2O_3 (Fig. S7c).

FT-IR spectra of the composites are given in Fig. S8a,b† The band at 1150 and 1017 cm^{-1} were assigned to asymmetric stretching vibration Al-O-Si, while 791 and 450 cm^{-1} were allocated to symmetric stretching and bending vibration of Al-O-Si. Sn impregnated composites have been shown the characteristic peaks at 592, 915, and 1627 cm^{-1}. Al impregnated composites have been given a characteristic peak at 1110 cm^{-1}. The peak observed at 460 cm^{-1} was indicated the Si-O bending vibration, and at 580 cm^{-1} was originated due to the double six-membered ring structure of the ZE [25]. All the composites have been displayed a distortion in between the 910-950 cm^{-1}, which is allocated to asymmetrical stretching of Si-O-M(M: Al or Sn). Sn-B-YZE and Al-B-YZE composites were shown bands at 3434, 3227, and 2260 cm^{-1}, which were arisen due to stretching vibration of SiO-H, BO-H, and B-OH, respectively. The B-OH bending vibration was assigned at 1187 cm^{-1}[20]. Whereas, these bands are completely absent in Al-B-NaYZE and Sn-B-NaYZE composites. The stretching and bending vibration of Si-O-B (borosilicate linkage) are observed at 927 and 649 cm^{-1}, respectively (Fig. S8a,b). In addition, the composites were incorporated B in the crystal lattices in the form of trigonal as well as tetrahedral valency states [22]. Thus, tetrahedral B was assigned the peak at 920-930 cm^{-1}, whereas trigonal B was at 1395 cm^{-1}.

Nitrogen adsorption-desorption was carried out to determine the SA and pore volume. The isotherms are investigated at a relative pressure of P/Po ranging from 0 to 0.9 (Supplementary Fig. S9a,b). The SA is calculated using Eq. (4), the SA, pore-volume, and pore radius are presented in Table 3.

$$SA = \frac{Vm}{22400} \times Am \times N \times 10^{-2} \quad (4)$$

Where SA: Surface area m^2/g, Vm: Volume of monolayer m^3, Am: Area occupied by one molecular of nitrogen in monolayer is 0.162 nm^2, N: Avogadro's number of a mole (6.02×10^{23} molecules).

The N_2 adsorption reveals that Al/Sn-B-Na-YZE belongs to type-1 isotherm and Al/Sn-B-YZE composite belongs to type-IV isotherm (Fig. S9a,b). Isotherms of NaYZE and Al/Sn-B-NaYZE exhibited microporous adsorption behavior as missing hysteresis loops within the framework, and the pattern of pore size distribution was indicated the lack of mesoporous behavior, which thereby confirmed the microporous nature. While, the isotherms of YZE and Al/Sn-B-YZE indicated the presence of some mesopores, due to the presence of hysteresis loop in the framework. The isotherm was raised at a low-pressure range with an increase in relative pressure (P/Po), and on further increasing the relative pressure the N_2 adsorption was increased, which confirmed the presence of mesopores in the composites [21]. The small change in SA and micropore volume after adsorption of Sn and Al indicated the successful incorporation of Sn and Al on ZE (NaYZE and YZE) (Table 3). Whereas, the significant decrease in SA and micropore volume was recorded when B was incorporated into the Sn-NaYZE framework which might be formed complex oxides of metal-Na-B. It is

interestingly observed that the Sn-B-NaYZE and Al-B-NaYZE have very low BET SA (18.4, 4.3 m^2g^{-1}), Langmuir SA (28.4, 6.9 m^2g^{-1}), total pore volume (0.022, 0.006 cm^3g^{-1}) with improved pore diameter (503.4, 583.8A^o), respectively. On the other hand, 1%Pd or 1%Ru reduced catalysts are prepared using inexpensive AC as a major percentage, which gave improved SA and porosity for enhancing the activity (Table 3).

Composites have been shown thermo-stability behavior up to 1000 ^oC (Fig. S10). The total mass losses of composites such as Sn-B-NaYZE, Al-B-NaYZE, Sn-B-YZE, and Al-B-YZE were 3.5%, 5.2%, 4.1%, and 6.7%, respectively in the entire temperature range, which indicated prepared catalysts were thermally more stable as compared to the respective base materials. The difference in the stability of base material catalyst and the metal incorporated base material catalyst is due to hinderance in diffusion of components by the incorporated metals, also hindering the phase transition kinetics. It was validated that Na was firmly associated with the composites to give extra stability and helped to generate the acidic sites. The phase transition kinetics is shown by the TGA evaluation of composites before and after Py adsorption (Fig. S11). The initial mass loss after Py adsorption was attributed to desorption from weakly acid sites, and the mass loss at a higher temperature (>400 ^oC) was attributed to desorption at strongly acidic sites up to 700 ^oC, which was well correlated the findings of NH_3-TPD result.

Metal loadings of the composites are determined by ICP-OES and SEM-EDX (Table 2, Table S5). The composites are contained the rational percentage of Al, Sn, Na, and B, which formed the complex architecture. Therefore, the reduction of SA and pore volume may be due to the partial pore blockage of ZE with these complex oxides [24]. It is justified that the drastic reduction (>50 times) of micropore volume and also the SA in Sn-B-NaYZE and Al-B-NaYZE (Table 3). But, the pore diameter (503.4-583.8 A^o) of the above composites was enhanced more than two times.

Carbonyl-ene rearrangement of citronellal

The carbonyl-ene rearrangement of citronellal is studied in Al-B-NaYZE, Sn-B-NaYZE, Al-B-YZE, and Sn-B-YZE composites (Scheme 2). Among these, Al-B-NaYZE and Sn-B-NaYZE are shown better activity (Table S2). Order followed by the catalytic activity of prepared composites are in this form Sn-B-NaYZE > Al-B-NaYZE > Sn-B-YZE > Al-B-YZE. Further, the elemental ratios of both these composites have been optimized for getting higher citronellal cyclization. The ratios of Sn-B-NaYZE (0.02:0.05:0.5) and Al-B-NaYZE (0.01:0.05:0.45) are optimum for performing a better activity (Fig. 3). This transformation has been studied in $CHCl_3$, CH_2Cl_2, and cyclohexane. It has been observed that cyclohexane gave 96% conversion of citronellal to about 98% of isopulegol isomers in 2 h at 70 ^oC (Fig. S12). The kinetics of transformation from citronellal to isopulegol has been optimized to obtain maximum conversion in 2 h (Fig. S13).

For a greener approach, the above chemical kinetics was studied over liquid-CO_2 medium for 60 min. There is 99% conversion of citronellal to about 99% of selectivity towards isopulegol isomers is attained in 45 min (Fig. 4a,b). Sn-B-NaYZE have been shown promising results with atmost enantioselectivity to (-)-isopulegol (Table 4). The enantiospecific analysis was revealed (-)-isopulegol (94%), (+)-neoisopulegol (3%), (+)-neoisoisopulegol (2%), and (+)-isoisopulegol (1%) from (+)-citronellal. Thus, the present composites have lower SA, but improved pore diameter and strong acidic character, which facilitated the exceptional conversion rate and selectivity to isopulegol. From the HRTEM image, it was observed that the Sn preferred spherical layer

type of arrangements in Sn-B-NaYZE with lattice planes distance in between 0.25-0.35 nm to facilitate the carbonyl-ene rearrangement. The reaction probably took place on Lewis and Bronsted acidic sites of the composites leading to a protonated citronellal, which is further transformed to more stable carbocation via intermolecular rearrangement followed by deprotonation to isopulegol (Scheme S2a). Further, the experimental figures obtained against logarithmic of reactant concentration vs time revealed that the reaction is followed by first-order kinetics (Fig. 4e). Therefore, the reaction was dependent on the initial concentration of citronellal, and the decrease of concentration was measured along with the progress of the reaction. As displayed, both the composites are associated with trigonal and tetragonal geometry, and there is a high possibility for the effective and selective transformation of carbonyl-ene rearrangement to isopulegol (Fig. 5). The present catalytic synthesis was equally effective for the conversion of either (+)-citronellal or its racemic mixture. Similarly, the developed composites were not only selective and efficient for the conversion of pure citronellal, but they were also equally effective in citronellal-rich essential oils.

Table S8, shows the comparison of catalyst activity in cyclization of citronellal to isopulegol with reported literature. All the works were reported the conversion in organic solvent medium with poor (%) enantioselectivity to (-)-isopulegol. While in our process, we have utilized the greener approach (liquid CO_2 medium) and a novel catalyst which is giving the prominent transformation of citronellal (99%) to enantiospecific (-)-isopulegol (95%) at a moderate reaction condition. Further these isoulegol isomers were utilized to produce menthol isomers (98%).

Reduction of isopulegol isomers

For reduction of isopulegol isomers, a different metal doped activated carbon catalysts were prepared and utilized at fixed reaction condition inorder to screan out the effective one (Fig. S1). Among, 1%Pd/AC and 1%Ru/AC catalysts were shown the better activity. Furhter, the effect of temperature and pressure are studied, and the results are listed in Table S4. The kinetics of reaction and distribution of menthol enantiomers with time using 1%Pd/AC and 1%Ru/AC catalysts are presented in Fig. 6. This reduction was attained by 99% conversion of isopulegols to menthols in 1 h at 60 ^{o}C and 40 psi H_2 pressure using 1%Pd/AC with 98% selectivity towards (±)-menthol. While, in case of 1%Ru/AC catalyst the conversion percentage of isopulegol was quite comparable but the selectivity to (±)-menthol isomers was reduced. From the comparative study, it was noticed that the high metal loading and high temperature lead to enhance the yield of un-desirable menthol isomers. Therefore optimized temperature, pressure and catalyst loading not only helped in conversion efficiency but also lead the pathway for semi-synthesis of enantiospecific (-)-menthol.

Composites activity

The rearrangement (Prins reaction) of citronellal to isopulegol is the rate-limiting step (Fig. 4e). These composites were associated with both Lewis and Bronsted acid sites, which facilitated the cyclization of citronellal. The composites comprised of Al, Si, and Sn were provided Lewis acid sites and properly coped with B for the generation of Bronsted acid sites. Composites prepared using different ratios of Al/Sn, YZE/Na-YZE, B have been studied for the conversion of citronellal to isopulegol (Fig. 5, Table S1). The results showed that 0.5-1.0%B and 4-6% of Al/Sn in YZE/NaYZE are effective combinations for the conversion of citronellal to isopulegol (Table S1). The composites Sn-B-NaYZE and Al-B-NaYZE have been shown the best catalytic

activity. Most likely, these two composites are oriented towards trigonal and tetragonal geometry as presented in Fig. 5a, which may facilitate the enhancement of the Lewis and Bronsted acidity. Therefore, these composites followed a peculiar mechanism in which both the trigonal and tetragonal configured species are actively participated in a complex form to show exceptional selectivity towards the cyclization of citronellal (Fig. 5b). Finally, the composites associated with high Lewis and Bronsted acidity, trigonal and tetragonal Metal-Na-B architecture, and improved pore diameter were facilitated the composite activities towards the Prins rearrangement.

Metal impreginated ZE were effective catalysts for monoterpene valorization [26,27]. Azkaar et al [26]. utilized Ru/H-beta-300 extrudates catalyst for citronellal conversion in a continuous flow reactor and they had obtained 67-73% of (-)-menthol. Maki-Arvela *et al* [9]. reported the isopulegol dimers (di-isopulegyl ethers) in the process of cyclization, but the present composites are very selective towards isopulegol without any unwanted dimers. Whereas in current process, the total 98% conversion to menthol isomers is attanined with 95% of enantioselectivty to (-)-menthol.

Enantiomeric selectivity and enrichment of (-)-menthol

The reaction was carried out with two substrates as (+)-citronellal and (±)-citronellal. The possible isopulegol enantiomers identified after completion of reaction are presented in Scheme S2b. (+)-Citronellal is found to transform 94% (-)-isopulegol as a major enantiomer. The other unfavorable diastereomers viz., (+)-neoisopulegol (3%), (+)-isoisopulegol (2%), and (+)-neoisoisopulegol (1%) are detected in trace (Fig. S14). These isopulegol enantiomers are transformed to the corresponding menthol (step 2) by reduction reaction (Fig. 7). Therefore (+)-citronellal was identified as an ideal substrate for the production of (-)-menthol in a two-step process (Scheme S3a). Menthol enantiomers obtained from the pure citronellal as well as from eucalyptus and citronella oils are estimated using chiral-GC-FID analysis. Menthol possesses eight diastereomers (four pairs of enantiomers) like (±)-menthol, (±)-isomenthol, (±)-neoisomenthol, and (±)-isoisomenthol (Fig. 7). But, (-)-menthol is the only pharmaceutically active enantiomer, which is accumulated by the Mentha plant through a biosynthetic enzymatic pathway [6]. But, this green processed (-)-menthol is further purified through derivatization. In the present process, menthyl acetate derivatives of all isomers of menthol have been prepared. But, only (-)-menthyl acetate is crystallized at 35 ^{o}C (Scheme S3b). This selective crystallization is achieved due to the structural orientation of (-)-menthyl acetate as presented in Scheme S3c. The (-)-menthyl acetate was followed a suitable chair conformer, where all bulky groups preferred to be equatorial in position; hence, the crystallization was easily attained. Whereas, (+)-menthyl acetate revealed the bulky groups in the axial position, hence the crystallization is difficult. Finally, (-)-menthyl acetate is hydrolyzed to obtain (-)-menthol as presented in Scheme S3b. This methodology was followed for the isolation of crude menthol (13 g) from Eucalyptus oil. After enrichment, the yield of (-)-menthol was 6 g. Similarly, the isolated yields of crude menthol and (-)-menthol were 5 g and 4 g from citronella oils, respectively. Therefore, citronella oil is a better substrate for the semi-synthesis to (-)-menthol as compared to the eucalyptus essential oil (Fig. 7).

NMR study of natural and synthetic menthol

(-)-Menthol, sourced from semi-synthesized essential oils (present process) and also from the petrochemical origin (synthetic available in the market) have been displayed in the same ^{13}C-NMR spectra. ^{13}C-NMR (δ) 31.6 (C-1), 45.1 (C-2), 71.6 (C-3), 50.2 (C-4), 23.2 (C-5), 34.6 (C-6), 22.2 (C-7), 25.9 (C-8), 16.1 (C-9), 21.0 (C-10) (Supplementary Fig. S15a,b). From the DEPT study, it is found that C-2, C-5, and C-6 are secondary carbon and others are either primary or tertiary carbons (Fig. S15c†). It is clear that menthol from natural (essential oil) and synthetic (petrochemical origin) (-)-menthol cannot be differentiated by chiral-GC-FID and NMR analyses.

Biobased index

The enantiomers of menthol are differentiated by Chiral-GC-FID and ^{13}C-NMR, however, the ^{14}C-radiocarbon analysis of synthetic (petrochemicals) and natural (-)-menthols are expected to give dissimilar biobased index (^{14}C content). The bio-based index (100%) of the isolated (-)-menthol is shown a higher pMC value (>99%), and it is very close to the menthol obtained from the *M. arvensis* essential oil. On the other hand, the synthetic menthol prepared by the chemical industry from petrochemicals has been shown a biobased value of 0% (Table 5). This is an interesting report on origin authentication of (-)-menthol using ^{14}C-radiocarbon-dating to validate as nature identical.

Chemical compositions and volatility of modified essential oil

The geraniol in citronella oil is partially transformed to dihydro-citronellol (Scheme 4a). In the process of catalytic modification, the partial reduction of geranyl acetate and citronellyl acetate to 3,7-dimethyloctyl acetate, 2,7-dimethylheptanol, etc is noticed (Scheme 4b). The catalytically modified oil was frozen (-40 ^{o}C) to crystallize the menthol. In addition, the spent oil contained only 13-15% menthol in dissolution state, and it is hardly crystallized due to its lower concentration. After isolation of menthol, the spent oil was enriched with other terpene alcohols (d-terpineol, terpinen-4-ol, a-terpineol, dihydro-citronellol, citronellol, geraniol), terpinyl acetate (3,7-dimethyloctyl acetate, citronellyl acetate, geranyl acetate), and sesquiterpenoids (9.8-1.5%). Interestingly, spend citronella oil was contained enrich percentage of (-)-citronellol (13.5-14.4%) and (-)-menthol (14.0-14.2%) along with linalool (1.8-1.9%), dihydro-citronellol (7.0-7.5%), geraniol (14.5-15.1%), 3,7-dimethyloctyl acetate (3.4-3.9%), citronellyl acetate (5.0-5.9%) and geranyl acetate (4.4-4.5%) are an ideal combination for improving olfactometry profile. This oil has smelled refreshing, rosy, and peppermint type with a cooling sensation. In general practice, isolation of (-)-menthol from *M. arvensis* essential oil, the remaining spent oil known as dementholized oil (DMO) contained 14-18% of menthol are very much in use where a low percentage of menthol is desired [5,6]. In terms of mentha oil trade, menthol crystal and DMO are equally important. Citronella essential oil contained only 38.9-41.4% of citronellal along with geraniol (20.8-21.8%), citronellol (9.9-10.0%), citronellyl acetate (4.0-4.2%), geranyl acetate (4.2-4.6%), elemol (4.2-5.1%), etc (Table 1). In the process of catalytic transformation, the above terpenoids were partially rearranged or reduced to comparatively higher volatile compounds (Scheme S4). As a result, the volatility of modified oils has been increased. Therefore, the chemical compositions are fully complying with the TGA and DTG results (Fig. S16).

From Fig. S16, the eucalyptus essential oil has displayed high volatility as compared to its modified oil. The high volatile isopulegol (10.9%) and citronellal (69.5%) are transformed to crystalline menthol (Table 1). The partial isolation of menthol as crystal was led to enhancement of the concentration of other constituents in the spent oil marked by 1,8-cineole (1.3%), d-terpineol (8.9%), a-terpineol (1.8%), terpinen-4-ol (5.9%), menthol

(13.1%), citronellol (15.5%), geraniol (1.2%), citronellyl acetate (9.8%), b-caryophyllene (9.7%) and b-caryophyllene oxide (1.2%) might be responsible for enhancing the olfactometry value. Similarly, the modified oil was appended structurally related compounds such as 2,6-dimethyl heptanol (1.8-1.9%), dihydro-citronellol (7.0-7.5%), and 3,7-dimethyl octyl acetate (3.4-3.9%) due to the process of catalytic transformation (Table 1, Scheme S4). Therefore, it has been displayed a better fragrance profile due to menthol along with the above bioactive terpene alcohols.

Anti-microbial and anti-oxidant activities

In current investigations, moderate activity was exhibited by the eucalyptus oil against Gram-(+)-bacteria (*Staphylococcus aureu*s) and also fungus viz., *Candida albicans*. The activity displayed by the eucalyptus essential oil has been accredited to the synergistic impact of the two major compounds viz., citronellal (69.5%) and citronellol (5.3%) [28].Further, the antibacterial activity of essential oil is found to be enhanced when the isopulegol and citronellal are converted to menthol (79.5%) (Table S7a). This activity was significantly enhanced in the spent oil against the *S. aureuas* after the separation of menthol crystal. The partial isolation of menthol as crystal was led to an increase in the concentration of other compounds in the spent oil such as 1,8-cineole (1.3%), d-terpineol (8.9%), a-terpineol (1.8%), terpinen-4-ol (5.9%), menthol (14.1%), citronellol (15.5%), geraniol (1.2%), citronellyl acetate (9.8%), b-caryophyllene (9.7%), and b-caryophyllene oxide (1.2%) might be responsible for enhancing the antimicrobial activities.

Citronella oils (CIM-Jeeva and BIO-13) were exhibited significant antimicrobial activities against *C. albicans, S. aureus,* and *S. typhimurium*. The observed activities in citronella oil were due to the presence of a majority of oxygenated terpenoid such as linalool (1.0-1.1%), citronellol (9.9-10%), geraniol (20.8-21.8%), citronellyl acetate (4.0-4.2%), geranyl acetate (4.2-4.6%), elemol (4.2-5.1%), a-cadinol (1.1-1.7%), etc [29]. The modified oil was appended structurally related compounds such as 2,6-dimethyl heptanol (1.8-1.9%), dihydro-citronellol (7.0-7.5%), and 3,7-dimethyl octyl acetate (3.4-3.9%) due to the process of catalytic transformation (Table 1, Scheme S4). Therefore, it has been displayed significant antifungal activity may be due to menthol along with the above bioactive terpene alcohols (Table S7b†). These spent oils are closed to the *M. piperita* essential oil, and are better suitable as a food-grade preservative without much altering the sensory value of the food products [1,3].

The antioxidant activity of the fresh essential oil, catalytically modified oil and spent oil of *C. citriodora*, CIM-Jeeva, and BIO-13 are shown in Fig. S17. For each of the three different essential oils, the modified and spent oil exhibit low IC: 50 values, and hence marked by high antioxidant activity in comparison to the fresh essential oils. The modified and spent oils have also shown high antioxidant activity at a concentration of 5 mg mL^{-1}. Menthol has been enhanced the activity in the modified and spent oil. A similar pattern in activities was observed at lower concentrations (2.5, 1.25, and 0.6 mg mL^{-1}) of all three essential oils.

Re-usability of catalyst

The reusailty of the heterogenous catalyst is the most promising feature of this conversion process. The isopulegol/menthol conversion rate for both the steps using Sn/Al-B-Na-YZE or 1%Pd/AC were stable upto four consecutive runs with only maxium 5% loss in yield indicating the high reusability potential of above catalysts, thereby making the overall process economical (Fig. 8). The reuse catalysts SAA, pore volume upto three

consecutive runs are presented (Table 6). Only some slight variation in SAA of reused catalyst was observed as compared to the fresh catalyst, which signified of their true hereogeneous nature of catalysts.

Conclusions

Al-B-NaYZE and Sn-B-NaYZE have displayed enhanced catalytic activity for carbonyl-ene rearrangement (Prins reaction) of citronellal to isopulegol, without formation of any isopulegol dimers. Composites were facilitated the enantiospecific semi-synthesis of isopulegol due to the formation of the complex (Na-B-Si-Al/Sn). The Al, Si, Sn were found responsible for the promotion of Lewis acidic sites, whereas the proper ratio of B facilitated the required trigonal and tetragonal coordinated composites to create Bronsted acidic sites. The advantage of Sn-B-NaYZE over the other composites was mainly due to the exceptional enhanced Lewis and Bronsted acidic properties along with $d^{3/2}$ and $d^{5/2}$ oxidation states. Further, Al-B-NaYZE and Sn-B-NaYZE have been shown very selective properties in terms of conversion of citronellal to isopulegol, which is a key rate-limiting step. The preparations of these composites are reported first time, where efficiency is maintained in five consecutive runs. Sn-B-NaYZE has displayed the distribution of Sn particles in spherical layers with its crystal lattice distance of 0.25–0.35 nm, this is further confirmed by calculating the *d*-spacing values of XRD data. The organic solvents were replaced by green solvent (liquid CO_2) for cyclization of citronellal at ambient temperature. In liquid-CO_2, the cyclization was completed in 45 min with better enantiospecificity. (+)-Citronellal was selectively converted to 99% of (-)-isopulegol in liquid-CO_2 (step-I), and it is further reduced by 1%Pd/AC to produce (-)-menthol of 98% purity in ethanol (step-II). It is demonstrated that the present process is effective for selective conversion of citronellal in essential oils to menthol. Menthol was easily isolated from the modified oils by the process of slow freezing to -40 ^{o}C. Further, esterification of racemic menthol mixture for obtaining (-)-menthyl acetate at 35 ^{o}C, followed by hydrolysis to acquire (-)-menthol. The isolated yield of (-)-menthol from *Eucalyptus* and *Citronella* essential oils was 30 and 20%, respectively.

Most importantly, our group has established a process to obtain flavor important (-)-menthol from low-value essential oils (fully citronellal transformation) directly using an environment-friendly and economical route up to 200 g scale for the first time. The liquid-CO_2 is a promising solvent due to its GRAS status, and conditions are maintained only by the cylinder pressure. This solvent is very much ideal for thermolabile terpenoids and gave enantiospecific (-)-menthol (> 90%) from citronellal. The present comprehensive semi-synthesis may have vast potential to fill the gap in demand of nature-identical (-)-menthol. This semi-synthesis (-)-menthol was proven to be nature-identical with 100% of the biobased index as compared to menthol sourced from petrochemical with almost zero morden carbon (< 1%). The modified oils, as well as the spent oils, have been displayed a better olfactometry profile along with the antioxidant activities, the residual oils are good alternative feedstocks for cosmeceutical applications. The spent oil is quite close to the *M. piperita* essential oil and can be used for flavoring food as well as a natural preservative without much altering the sensory value of the food products. The enrichment of minor terpene alcohols such as 1,8-cineole, terpinen-4-ol, α-terpineol, dihydro-citronellol, citronellol, citronellyl acetate, geranyl acetate, elemol, α-cadinol, etc in spent oils might be responsible for enhancing the olfactometry value and anti-oxidant activities. This is a complete, novel, green, low operating condition, and short time process for the value addition of citronellal in the

essential oil to nutraceutical and flavor important (-)-menthol. The spent oils may find diverse applications in the preparation of health care formulations with organoleptically superior products.

Abbreviations

AC, Activated charcoal; **ZE,** Zeolite; **NaYZE,** Na-Y-Zeolite; **YZE,** Y-H-Zeolite; AMS, Accelerator Mass Spectrometry; **pMC,** Percentage of modern carbon; **AGE,** Automated graphitization equipment; **EU,** *Corymbia citriodora;* **CIM**-J**eeva,** CIM-Jeeva, A variety of citronella; BIO-13**,** A variety of citronella; **EU-1,** Fresh eucalyptus oil; **EU-2,** Modified eucalyptus oil; **EU-3,** Spent eucalyptus essential oil; **CNJ-1,** Fresh citronella jeeva oil; **CNJ-2,** Modified Jeeva oil; **CNJ-3,** Spent Jeeva essential oil; **CNB-1,** Fresh citronella Bio-13 oil; **CNB-2,** Modified Bio-13 essentia oil; **CNB-3,** Spent bio-13 essential oil; SA, *Staphylococcus aureus* (MTCC96); ST, *Staphylococcus typhimurium* (MTCC43232); ATCC, *Candida albicans* (14053); MIC, Minimum inhibitory concentration; ZOI, Zone of inhibition.

Declarations

Data availability Statement

Data are available and a part a data are summarized as Supplementary materials

Declaration of interests

The authors declare that they have no known competing financial interests or personal relationships that could have appeared to influence the work reported in this paper.

Acknowledgments

The authors are thankful to Science and Engineering Research Board (SERB), DST, India (CRG/2021/002525) for research funding. We are grateful to Director, CSIR-CIMAP, Lucknow for providing the necessary facility under Aroma Mission, Phase-II (HCP 0007). Authors are thankful to IUAC for extending the AMS facility for ^{14}C funded by the Ministry of Earth Science (MoES), Govt. of India with reference numbers MoES/16/07/11(i)-RDEAS and MoES/P.O.(Seismic)8(09)-Geochron/2012.

References

1. dos Passos Braga, S., Magnani, M., Madruga, M.S., de Souza Galvão, M., de Medeiros, L.L., Batista, A.U.D., Dias, R.T.A., Fernandes, L.R., de Medeiros, E.S., de Souza, E.L.: Characterization of edible coatings formulated with chitosan and mentha essential oils and their use to preserve papaya (*Carica papaya* L.). **Innov. Food Sci. Emerg. Technol. 2020,** 65, 102472.
2. Santos, M.G., Carpinteiro, D.A., Thomazini, M., Rocha-Selmi, G.A., da Cruz, A.G., Rodrigues, C.E., Favaro-Trindade, C.S.: Coencapsulation of xylitol and menthol by double emulsion followed by complex coacervation and microcapsule application in chewing gum. **Food Res.Int.** 2014, **6**, 454-462.
3. Guerra, I.C.D., de Oliveira, P.D.L., Santos, M.M.F., Lúcio, A.S.S.C., Tavares, J.F., Barbosa-Filho, J.M., Madruga, M.S., de Souza, E.L.: The effects of composite coatings containing chitosan and Mentha

(*piperita L*. or x *villosa Huds*) essential oil on postharvest mold occurrence and quality of table grape cv. Isabella. **Innov. Food Sci. Emerg. Technol. 2016,34**, 112-121.

4. Suankaew, N., Matsumura, Y., Saramala, I., Ruktanonchai, U.R., Soottitantawat, A., Charinpanitkul, T.: L-Menthol crystal micronized by rapid expansion of supercritical carbon dioxide. J. Ind. Eng. Chem. 2012, 18, 904-908.
5. Egan, M., Connors, É.M., Anwar, Z., Walsh, J.J.: Nature's Treatment for Irritable Bowel Syndrome: Studies on the Isolation of (−)-Menthol from Peppermint Oil and Its Conversion to (−)-Menthyl Acetate. J Chem. Educ. 2015, 92, 1736-1740.
6. Chanotiya, C.S., Pragadheesh, V.S., Yadav, A., Gupta, P., Lal, R.K.: Cyclodextrin-based gas chromatography and GC/MS methods for determination of chiral pair constituents in mint essential oils. J. Essent. Oil Res. 2021, **33**, 23-31.
7. Prakash, O.M., Naik, M., Katiyar, R., Naik, S., Kumar, D., Maji, D., Shukla, A., Nannaware, A.D., Kalra, A., Rout, P.K..: Novel process for isolation of major bio-polymers from Mentha arvensis distilled biomass and saccharification of the isolated cellulose to glucose. **Ind. Crops Prod. 2018, 119**, 1-8.
8. Guo, Y., Gaczyński, P., Becker, K.D., Kemnitz, E.: Sol-Gel synthesis and characterisation of nanoscopic FeF_3-MgF_2 heterogeneous catalysts with bi-acidic properties. ChemCatChem. 2013, 5, 2223-2232.
9. Mäki-Arvela, P., Kumar, N., Nieminen, V., Sjöholm, R., Salmi, T., Murzin, D.Y.: Cyclization of citronellal over zeolites and mesoporous materials for production of isopulegol. J Catal. 2004, 225, 155-169.
10. Itoh, H., Maeda, H., Yamada, S., Hori, Y., Mino, T., Sakamoto, M.: Highly selective aluminium-catalysed intramolecular Prins reaction for l-menthol synthesis. RSC Adv. 2014, 6, 61619-61623.
11. Rout, P.K., Rao, Y.R., Naik, S.: Liquid CO_2 extraction of *Murraya paniculata* Linn. flowers. **Ind Crops Prod. 2010, 32**, 338-342.
12. Sharma, R., Umapathy, G.R., Kumar, P., Ojha, S., Gargari, S., Joshi, R., Chopra, S., Kanjilal, D.: Ams and upcoming geochronology facility at inter university accelerator centre (IUAC), New Delhi, India. Nucl. Instrum. **Methods** Phys. Res. **B. 2019,** 438, 124-130.
13. Xie, Y., Wang, K., Huang, Q., Lei, C.: Evaluation toxicity of monoterpenes to subterranean termite, Reticulitermes chinensis Snyder. **Ind. Crops Prod. 2014,** 53, 163-166.
14. Ramezani, H., Azizi, S.N., Hosseini, S.R.: NaY zeolite as a platform for preparation of Ag nanoparticles arrays in order to construction of H_2O_2 sensor.Sens. Actuators B Chem. 2017, **248**, 571-579.
15. Treacy, M.M.J., Higgins, J.B.: Collection of simulated XRD powder patterns for zeolites, 5th ed., Elsevier, Amsterdam 2007, 477-485.
16. Meng, B., Ren, S., Liu, X., Zhang, L., Hu, Q., Wang, J., Guo, Q. and Shen, B.: Synthesis of USY zeolite with a high mesoporous content by introducing Sn and enhanced catalytic performance. **Ind. Eng. Chem. Res. 2020,** 59, 5712-5719.
17. Robson, H., Lillerud, K.P.: Verified synthesis of zeolitic materials, Second Rev, Elsevier Science B.V, Amsterdam 2001, **265**.
18. Zhou, N., Polavarapu, L., Wang, Q., Xu, Q.H. Mesoporous SnO_2-coated metal nanoparticles with enhanced catalytic efficiency. ACS Appl. Mater. Interfaces. 2015, 7-8, 4844-4850.

19. Pal, P., Das, J.K., Das, N., Bandyopadhyay, S.: Synthesis of NaP zeolite at room temperature and short crystallization time by sonochemical method. **Ultrason** Sonochem. 2013, 20, 314-321.
20. Parveen, M., Ahmad, F., Malla, A.M., Azaz, S.: SiO_2-H_3BO_3 promoted solvent-free, green and sustainable synthesis of bioactive 1-substituted-1-H-tetrazole analogues. New J. Chem. 2015, 39, 2028-2041.
21. Liao, J., Zhang, Y., Fan, L., Chang, L., Bao, W.: Insight into the acid sites over modified NaY zeolite and their adsorption mechanisms for thiophene and benzene. **Ind. Eng. Chem. Res. 2019,** 58, 4572-4580.
22. Ranoux, A., Djanashvili, K., Arends, I.W., Hanefeld, U.: B-TUD-1: a versatile mesoporous catalyst. RSC Adv. 2013, 3, 21524-21534.
23. Guan, F.F., Ma, T.T., Yuan, X., Zeng, H.Y., Wu, J.: Sn-modified NaY zeolite catalysts prepared by post-synthesis methods for Baeyer-Villiger oxidation. Catal. Lett., 2018, 148, 443-453.
24. Ali, S.A., Almulla, F.M., Jermy, B.R., Aitani, A.M., Abudawoud, R.H., AlAmer, M., Qureshi, Z.S., Mohammad, T., Alasiri, H.S.: Hierarchical composite catalysts of MCM-41 on zeolite Beta for conversion of heavy reformate to xylenes. J. Ind. Eng. Chem. Res. 2021, 98, 189-199.
25. Hammond, C., Padovan, D., Al-Nayili, A., Wells, P.P., Gibson, E.K., Dimitratos, N.: Identification of active and spectator Sn sites in Sn-β following solid-state stannation, and consequences for Lewis acid catalysis. ChemCatChem. 2015. *7*(20), 3322-3331.
26. Azkaar, M., Arvela, P. M. , Vajglová, Z., Fedorov, V., Kumar, N. , Hupa, L., Hemming, J., Peurla, M., Ahoa, A. , Murzin, D. Y.: Synthesis of menthol from citronellal over supported Ru- and Pt-catalysts in continuous flow. React. Chem. Eng. 2019, 4, 2156.
27. Gupta, M., Kumar, P., Sharma, P.K., Chanotiya, C.S., Mohapatra, P., Rout, P.K.*:* Valorization of monoterpene hydrocarbon fraction of essential oil to high-value oxygenated monoterpenoids by solvent-free catalytic modification using 1%Pd-β-Zeolite. Waste Biomass Valor. 2022. Doi: 10.1007/s12649-022-01726-9.
28. Lopez-Romero, J.C., Gonzalez-Rios, H., Borges, A., Simoes, M.: Antibacterial effects and mode of action of selected essential oils components against *Escherichia coli* and *Staphylococcus aureus*. Evid **Based** Complement Alternat Med. 2015, **795435**, 1-9.
29. Elsharif, S.A., Buettner, A.: Influence of the chemical structure on the odor characters of citronellol and its oxygenated derivatives. Food Chem. 2017, **232**, 704-711.

Tables

Table 1 Compositions of citronella (CIM-Jeeva and BIO-13) and *C. citriodora* essential oils and their modified oils

Compounds	Essential oils			Modified oils			Spent oils			Identification
	EU	Jeeva	BIO-13	EU	Jeeva	BIO-13	EU	Jeeva	BIO-13	
α-Pinene	0.3	-	-	0.2	-	-	1.4	-	-	MS, RI
β-Pinene	0.8	-	-	0.6	-	-	2.5	-	-	MS, RI
2,6-Dimethylheptanol	-	-	-	-	1.5	1.0	1.5	1.9	1.8	MS
Myrcene	-	0.5	0.3	-	0.3	0.5	-	0.7	0.8	MS, RI
α-Terpinene	0.1	0.1	0.1	0.1	0.2	0.2	0.8	0.6	0.6	MS, RI
3-Menthene	-	-	-	-	3.2	4.1	-	4.2	4.4	MS, RI
Limonene	0.2	2.8	2.9	0.2	3.0	3.2	0.9	4.2	4.4	MS, RI
1,8-Cineole	0.2	-	-	0.2	-	-	1.3	-	-	MS, RI
(*Z*)-β-Ocimene	0.1	-	-	0.1	-	-	0.7	-	-	MS, RI
(*E*)-β-Ocimene	0.5	-	-	0.3	-	-	1.4	-	-	MS, RI
γ-Terpinene	0.3	0.1	0.1	0.3	0.1	0.1	1.9	0.5	0.4	MS, RI
p-Cymene	0.1	-	-	0.1	-	-	0.7	-	-	MS, RI
Terpinolene	-	0.1	0.1	-	0.3	0.2	-	0.9	0.8	MS, RI
Linalool	-	1.0	1.1	-	0.7	0.7	-	1.8	1.9	MS, RI
Isopulegol	10.9	-	-	0.3	0.1	0.1	0.8	0.2	0.3	MS, RI
Citronellal	**69.5**	**38.9**	**41.4**	0.4	0.3	0.3	0.7	0.6	0.5	MS, RI
Neo-isopulegol	-	-	-	-	0.2	0.2	0.5	0.4	0.3	MS, RI
δ-Terpineol	1.1	-	-	1.1	2.9	2.8	8.9	3.2	4.3	MS
Borneol	-	0.1	0.1	-	0.1	0.1	-	0.3	0.2	MS, RI
Menthol*	-	-	-	**79.5**	**38.2**	**41.2**	**13.1**	**14.2**	**14.1**	MS, RI
Terpinen-4-ol	0.8	-	-	0.8	-	-	5.9	-	-	MS, RI
α-Terpineol	0.2	-	-	0.2	1.2	1.0	1.8	2.1	2.1	MS, RI
Dihydro-citronellol	-	-	-	1.2	5.5	5.4	8.2	7.0	7.5	MS
Citronellol	5.3	10.0	9.9	4.5	9.0	8.5	15.5	14.4	13.5	MS, RI
Geraniol	0.2	**21.8**	**20.8**	0.1	12.2	11.6	1.2	15.1	14.5	MS, RI
Geranial	-	0.5	0.6	-	-	-	-	-	-	MS, RI
3,7-Dimethyloctylacetate	-	-	-	-	3.0	3.5	-	3.4	3.9	MS

Citronellylacetate	2.7	4.0	4.2	2.6	3.7	3.7	9.8	5.0	4.9	MS, RI
Geranyl acetate	0.2	4.2	4.6	0.2	3.6	3.4	1.1	4.5	4.4	MS, RI
β-Cubebene	0.1	-	-	0.1	-	-	0.9	-	-	MS, RI
β-Elemene	-	0.9	0.6	-	0.4	0.3	-	0.5	0.5	MS, RI
β-Caryophellene	2.3	0.1	0.1	2.3	0.2	0.2	9.7	0.4	0.5	MS, RI
g-Cadinene	-	0.2	0.2	-	0.3	0.3	-	0.5	0.5	MS, RI
β-Caryophelleneoxide	0.3	-	-	0.1	-	-	1.2	-	-	MS, RI
Elemol	-	5.1	4.2	-	4.9	3.9	-	6.3	5.5	MS, RI
α-Cadinol	-	2.0	1.2	-	2.2	1.0	-	3.2	2.8	MS, RI
Total	96.2	92.4	92.5	95.5	97.3	97.5	92.4	95.6	95.7	
Monoterpene hydrocarbons	2.4	3.6	3.5	1.9	7.1	8.3	9.3	11.1	11.4	
Oxygenated terpenoids	91.1	81.8	83.3	91.1	80.7	82.5	68.8	71.2	71.7	
Sesquiterpenoids	2.7	8.0	5.7	2.5	8.0	5.7	11.8	10.5	9.8	

EU: *Corymbia citriodora*; Jeeva: CIM-Jeeva, A variety of citronella; BIO-13, A variety of citronella; *Confirmed by NMR; Cyclodextrin phase is enantiomeric characterized the (-)-menthol and (-)-citronellol.

Table 2: Si/Al ratio and percentage of Na, Sn and B in the composites

Catalysts	Crystallinity %[a]	Si/Al ratio[b]	Weight %		
			Na (wt%)[b]	Sn (wt%)	B (wt%)[c]
NaYZE	85.6	2.74	5.04	-	-
YZE	88.9	2.86	-	-	-
Sn-B-NaYZE	92.4	2.47	5.71	3.74	0.98
Al-B-NaYZE	94.2	2.05	5.17	-	0.92
Sn-B-YZE	91.6	2.38	-	2.18	0.94
Al-B-YZE	92.5	2.14	-	-	0.95

a: XRD , b: SEM-EDX, c: XPS

Table 3: Characterization of surface area and porosity of catalysts

Catalyst	BET Surface area ($m^2 g^{-1}$)	Langmuir Surface area ($m^2 g^{-1}$)	Total Pore volume ($cm^3 g^{-1}$)	Average pore diameter (A^o)
NaYZE	626.3	1158.1	0.335	214.4
YZE	675.2	1128.3	0.468	277.4
Sn-NaYZE	415.6	616.5	0.242	233.6
Al-NaYZE	406.6	599.9	0.219	216.2
Sn-YZE	516.0	763.7	0.353	273.6
Al-YZE	671.3	998.6	0.481	286.6
Sn-B-NaYZE	18.4	28.4	0.022	**503.4**
Al-B-NaYZE	4.3	6.9	0.006	**583.8**
Sn-B-YZE	354.9	527.3	0.263	296.6
Al-B-YZE	408.8	603.6	0.305	298.6
1%Pd/AC	763.9	922.3	0.592	310.4
1%Ru/AC	752.9	1001.7	0.661	340.4

Table 4: Percentage of conversion and selectivity of (+)-citronellal in liquid CO_2 medium

Catalysts	Reaction rate (mmol min^{-1})	Conversion (%)	Enantioselectivity of (-)-isopulegol	Total isopulegol (%)
Al-B-NaYZE	0.0525	98	91	97
Sn-B-NaYZE	0.0525	99	93	99

Reactant concentration (citronellal) = 0.0064 moles, reaction time 45 min

Table 5: ^{14}C dating analysis (biobased index) of (-)-menthol

Menthol	pMC	Biobased index (%)
Present process (Essential oils)	99.654±0.355	100
Menthol isolated from Mentha essential oil	99.974±0.379	100
Synthetic menthol (market sample, petrochemical as substrate)	0.465 ±0.0191	0
Isopulegol (intermediate)	99.72±0.279	100

pMC: percentage of modern carbon

Table 6:. Comparison of the surface property of the fresh catalyst and reused catalysts via surface area analysis.

Sample code	BET SA (m^2 g^{-1})	Langmuir SA (m^2 g^{-1})	TPV (cm^3 g^{-1})	Avg. pore diameter (A°)
Sn-B-NaYZE (F)	18.4	28.4	0.022	503.4
Al-B-NaYZE (F)	4.3	6.9	0.006	583.8
Sn-B-NaYZE (1T)	16.9	27.4	0.019	489.9
Al-B-NaYZE (1T)	4.0	6.2	0.006	555.2
Sn-B-NaYZE (2T)	16.5	27.2	0.018	485.0
Al-B-NaYZE (2T)	3.8	5.9	0.005	545.1
Sn-B-NaYZE (3T)	16.1	26.6	0.018	483.9
Al-B-NaYZE (3T)	3.6	5.7	0.005	537.3
1%Pd/Ac (F)	763.9	922.3	0.59	310.4
1%Pd/Ac (1T)	750.2	908.4	0.56	300.2
1%Pd/Ac (2T)	744.4	900.1	0.54	297.1
1%Pd/Ac (3T)	736.2	891.6	0.53	294.1

F: fresh preparation, IT: After one time used, 2T: After two time used, 3T: After three-time used, TPV: Total pore volume

Figures

Figure 1

HRTEM images of Sn-B-NaYZE; (A) 50 nm (B) *d*-spacing value (at 5 nm), (C) SAED Pattern (D) HRTEM image of Al-B-NaYZE (E) Mapping image with elemental percentage (F-I) Individual mapping of elements of Sn-B-NaYZE composite (k) EDAX graphand of Sn-B-NaYZE.

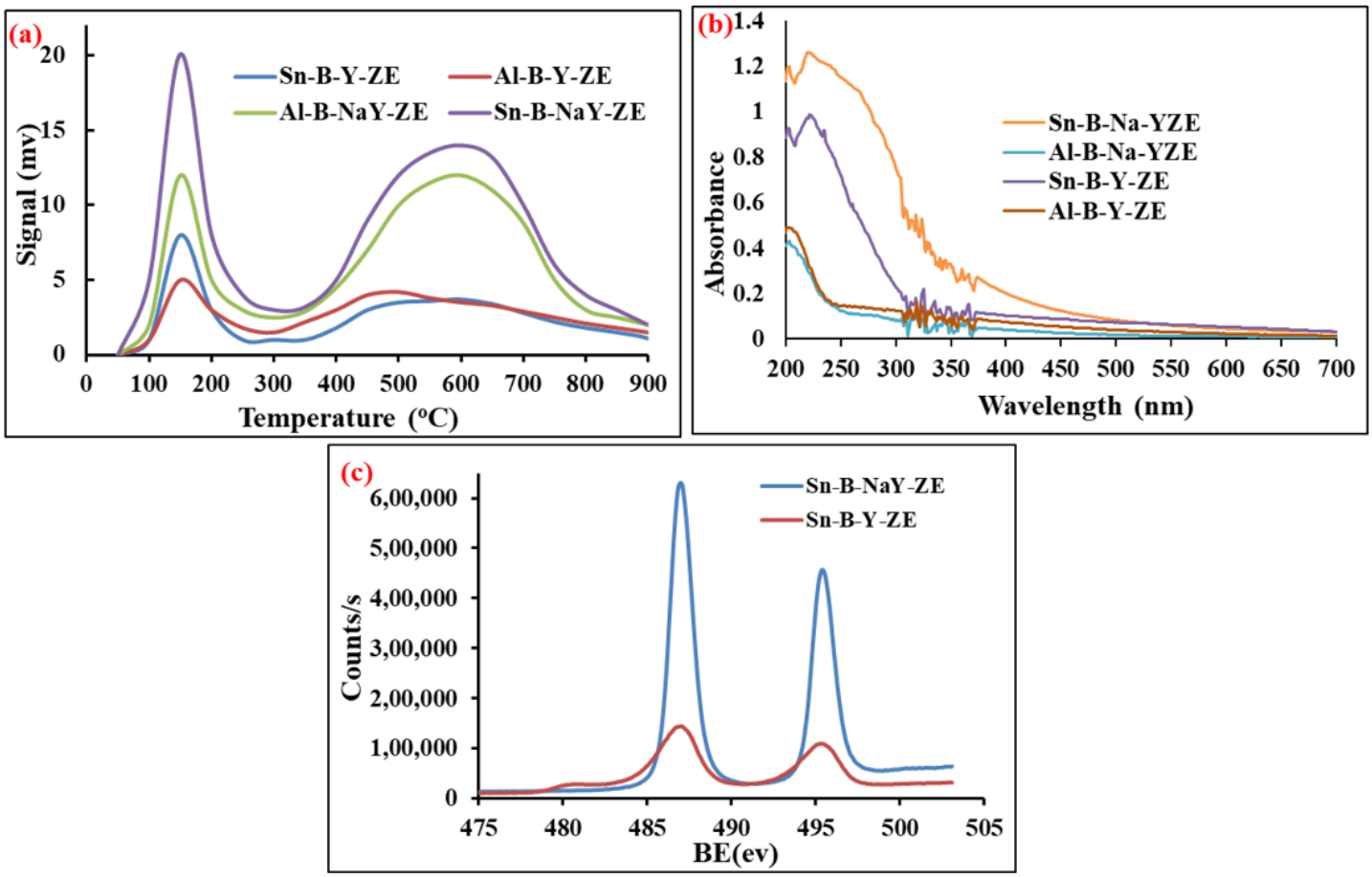

Figure 2

(a) NH_3-TPD analysis of catalysts Sn-B-NaYZE, Al-B-NaYZE, Sn-B-YZE and Al-B-YZE (b) Comparative UV-Vis spectra of composites Sn-B-NaYZE, Al-B-NaYZE, Sn-B-YZE and Al-B-YZE (c)Sn 3d spectra of Sn-B-NaYZE and Sn-B-YZE.

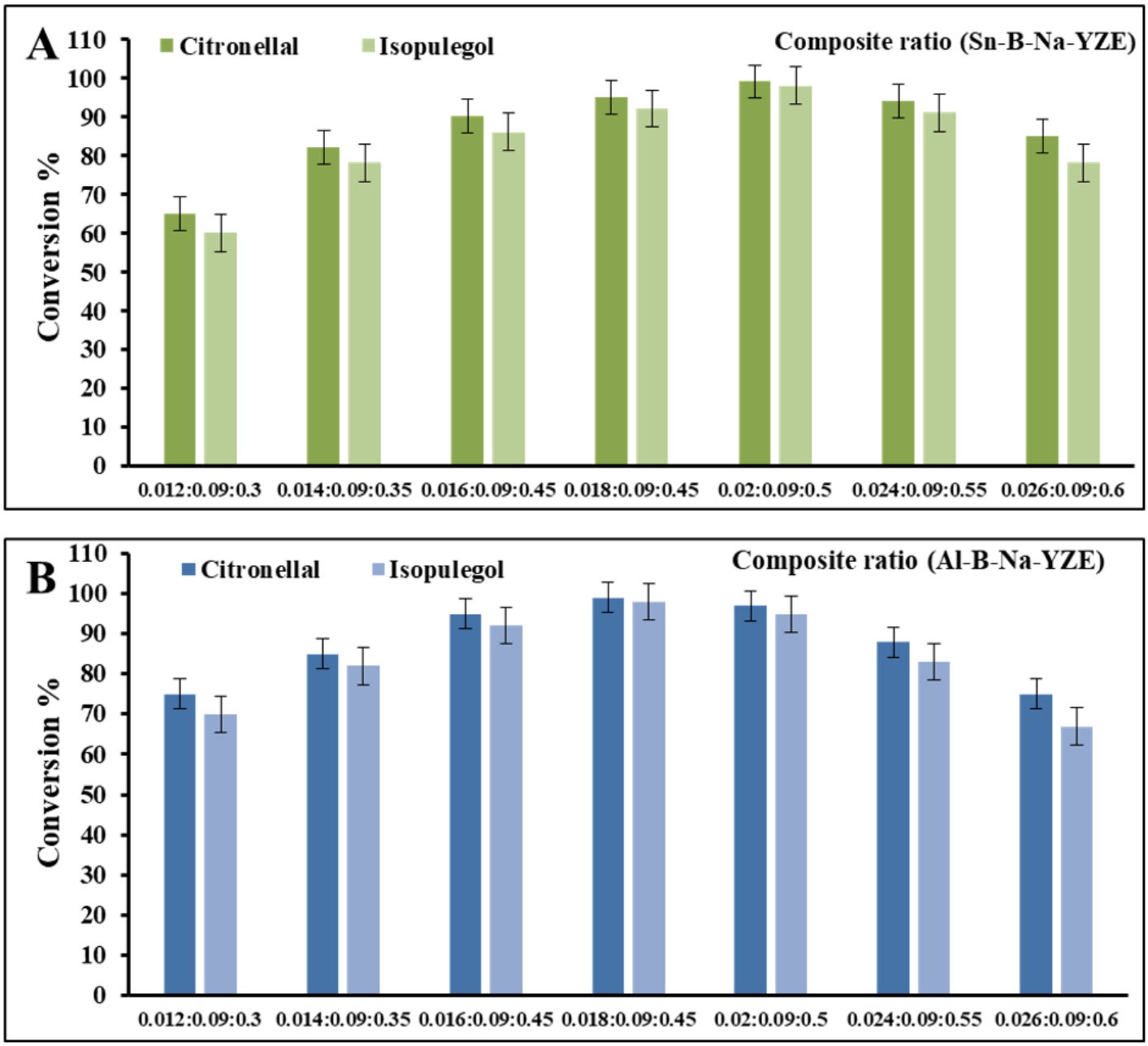

Figure 3

Mole ratio of components in the composites for conversion of citronellal to isopulegol (a) Sn-B-NaYZE, (b) Al-B-NaYZE

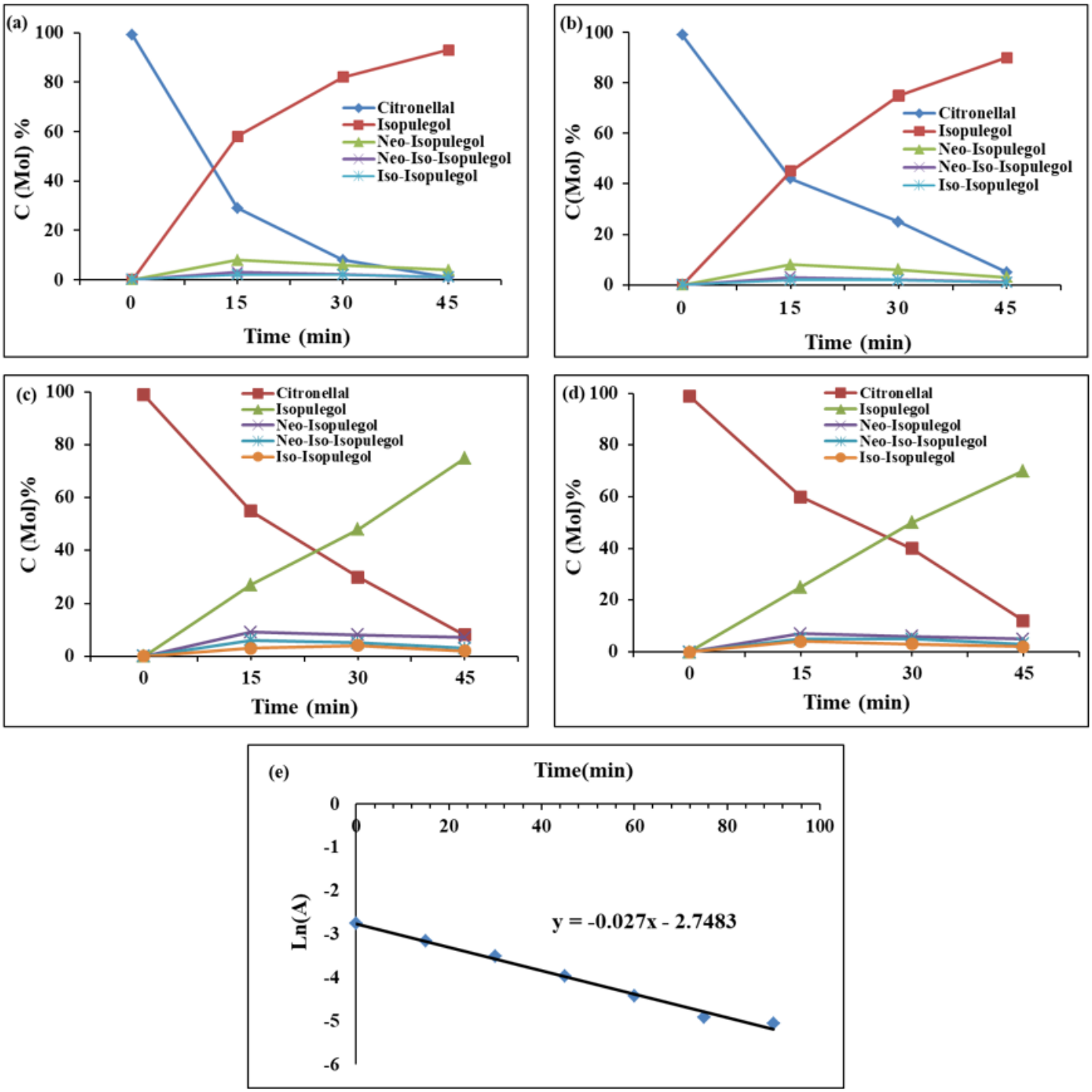

Figure 4

Kinetics of cyclization of citronellal to isopulegols (a) Sn-B-NaYZE, (b) Al-B-NaYZE,

(c) Sn-B-YZE, (d) Al-B-YZE, (e) Logarithmic of reactant concentration Vs time [A: citronellal]

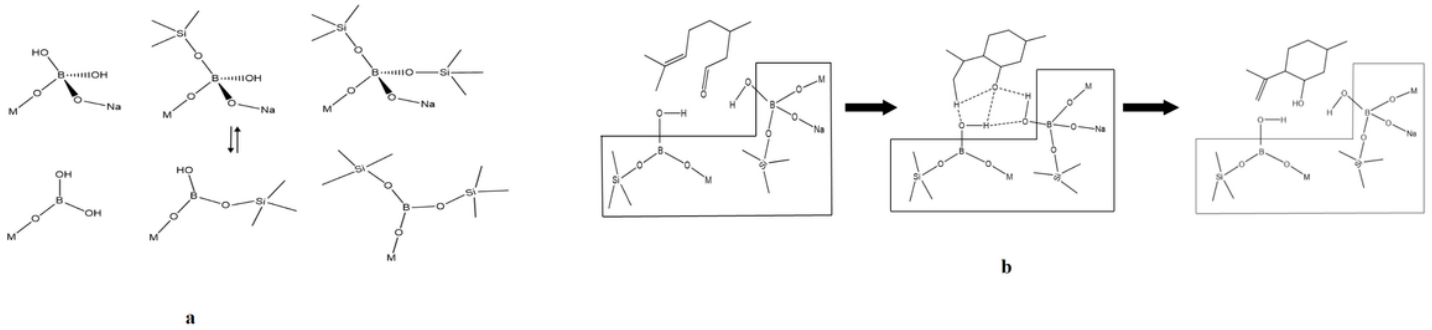

Figure 5

a Possible structure of trigonal and tetragonal geometry of composites (M: Al/Sn)

b Reaction mechanism involved using trigonal and tetragonal configurations (M: Al/Sn)

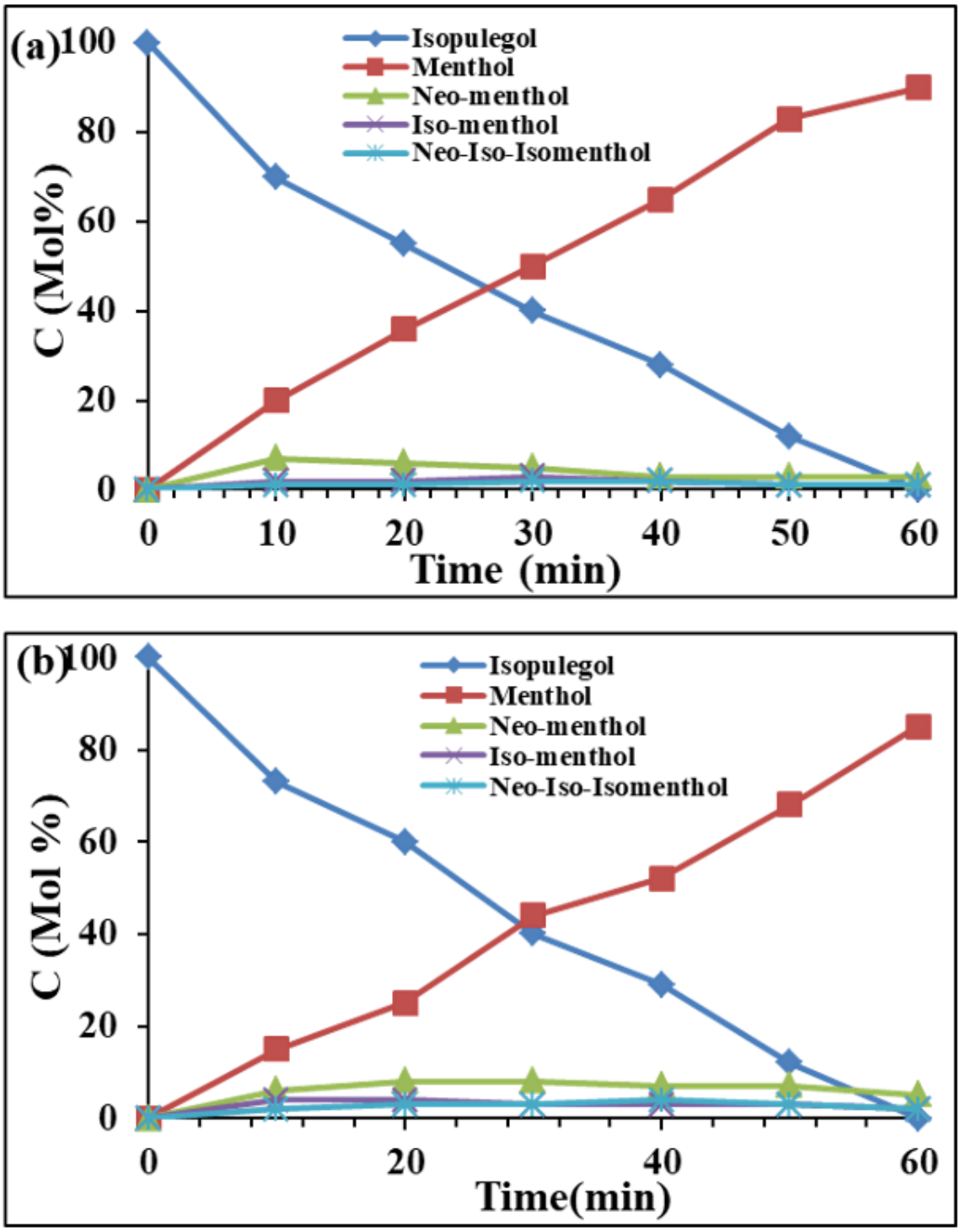

Figure 6

Kinetics of reduction of isopulegol to menthols (a)1%Pd/AC, (b) 1%Ru/AC

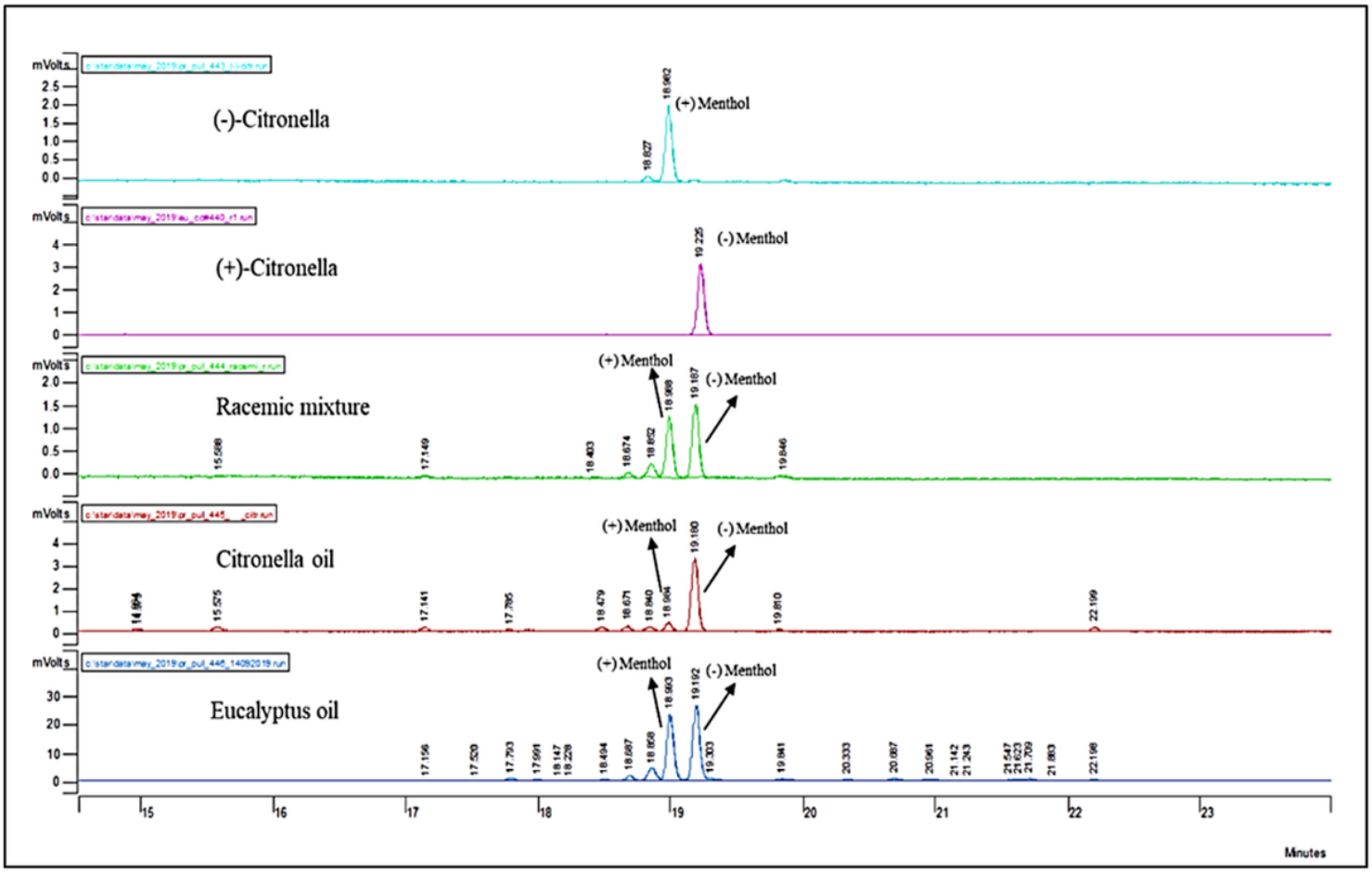

Figure 7

Comparative Chiral-GC-FID analysis of menthol isomers obtained from (+)-citronellal, (-)-citronellal, (±)-citronellal, citronella and eucalyptus essential oils

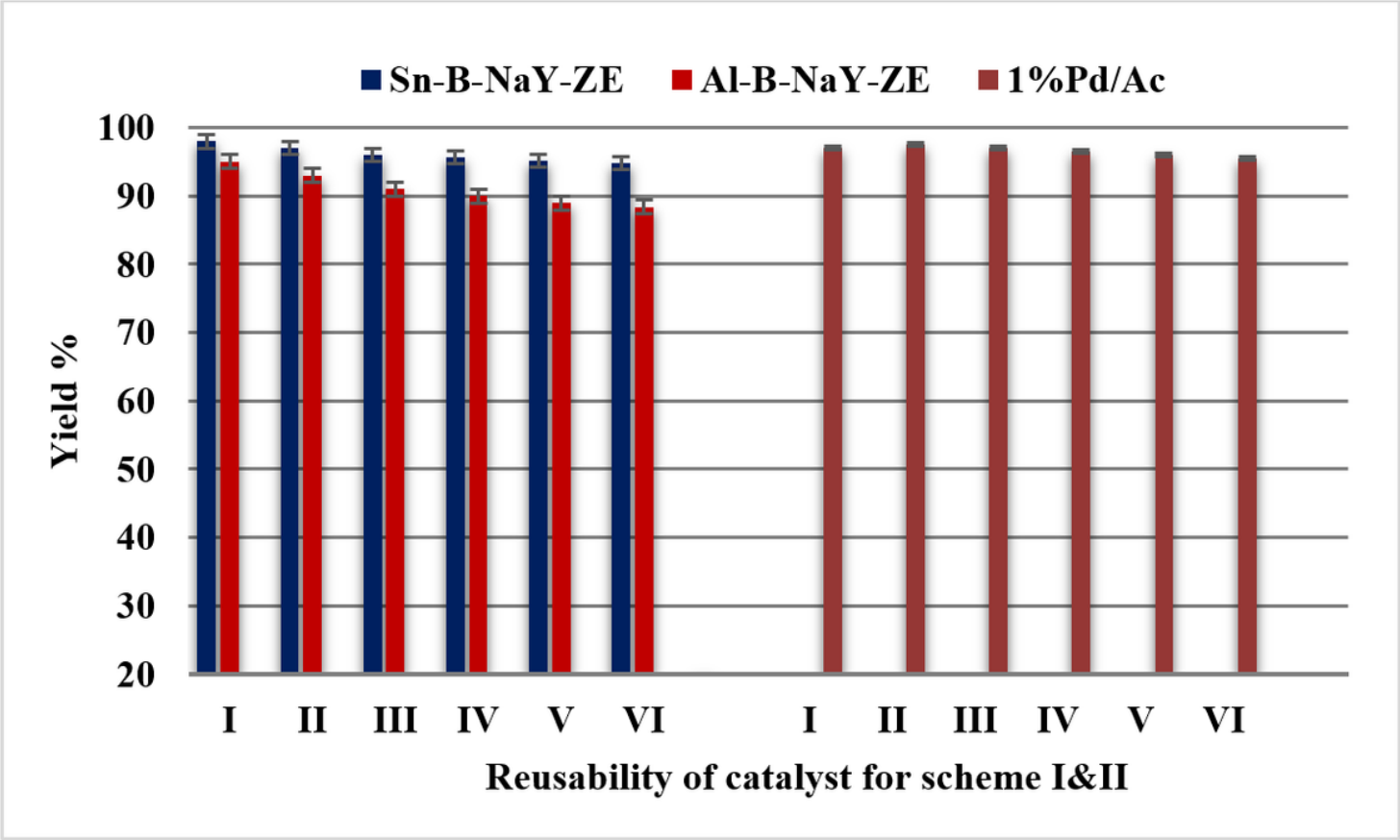

Figure 8

Yield (%) of product obtained by re-using the catalysts, (a) Sn-B-NaYZE, (blue) (b) Al-B-NaYZE,(red) (c) 1%Pd/AC (light red).

Supplementary Files

This is a list of supplementary files associated with this preprint. Click to download.

- Supplementaryinformation.docx